

Multiphase material topology optimization of Mindlin-Reissner plate with nonlinear variable thickness and Winkler foundation

Thanh T. Banh^{1a}, Xuan Q. Nguyen^{1b}, Michael Herrmann^{2,3c},
Filip C. Filippou^{2d} and Dongkyu Lee^{*1}

¹Department of Architectural Engineering, Sejong University, 209 Neungdong-ro, Gwangjin-gu, Seoul 05006, Republic of Korea

²Department of Civil and Environmental Engineering, University of California, Berkeley, CA 94720 United States of America

³Structure GmbH, 70176 Stuttgart, Germany

(Received October 17, 2019, Revised February 12, 2020, Accepted February 20, 2020)

Abstract. In typical, structural topology optimization plays a significant role to both increase stiffness and save mass of structures in the resulting design. This study contributes to a new numerical approach of topologically optimal design of Mindlin-Reissner plates considering Winkler foundation and mathematical formulations of multi-directional variable thickness of the plate by using multi-materials. While achieving optimal multi-material topologies of the plate with multi-directional variable thickness, the weight information of structures in terms of effective utilization of the material at the appropriate thickness location may be provided for engineers and designers of structures. Besides, numerical techniques of the well-established mixed interpolation of tensorial components 4 element (MITC4) is utilized to overcome a well-known shear locking problem occurring to thin plate models. The well-founded mathematical formulation of topology optimization problem with variable thickness Mindlin-Reissner plate structures by using multiple materials is derived in detail as one of main achievements of this article. Numerical examples verify that variable thickness Mindlin-Reissner plates on Winkler foundation have a significant effect on topologically optimal multi-material design results.

Keywords: multiphase material topology optimization; Mindlin-Reissner plate theory; variable thickness; mixed interpolation of tensorial components (MITC4); Winkler foundation

1. Introduction

Since the leader research by Bendsøe and Kikuchi (1988), topology optimization has made noteworthy progress as a creative numerical and design method, drawing an enormous amount of attention from scientific and engineering communities (Xu *et al.* 2012, Rozvany *et al.* 2002, Lee and Shin 2016, Vatanabe *et al.* 2016, Roodsarabi *et al.* 2016, Bagherinejad and Haghollahi 2018). One of the interesting issues which based on main ideas of standard topology optimization field is multi-material topology optimization. With the same goal of single material consideration with respect to achieving both higher structural stiffness and material cost savings, multi-material application gives a significant opportunity to add stiffer materials with the same amount of volume constraint.

Multi-material topology optimization also can be applied to optimize cellular structures like functionally graded concrete (FGC) (Herrmann and Sobek 2017). In the concept of FGC material density and therewith material stiffness is designed to fulfil the needs of the local stress state in the interior of a concrete component, saving up to 60% of dead weight in comparison to a homogeneous concrete beam. The authors are currently applying the multi-material topology optimization approach to FGC by allowing 5 to 7 predefined concrete mixes in the optimization. The hardened concrete properties of the mixes available during the optimization were previously experimentally determined. Therefore, the optimization results will always be physically feasible and do not need to be classified in material groups anymore, as it has been done before with a typical single material topology optimization approach (Bendsøe 1997). Sigmund and Torquato (1997) presented the three-phase topology optimization method for the design of materials with extreme thermal expansion. A method for the multi-material structural topology optimization with a generalized Cahn-Hilliard model is presented by Zhou and Wang (2007). Lieu and Lee (2017) proposed a novel multi-resolution scheme to perform the multi-material topology optimization in the framework of isogeometric analysis. Doan and Lee (2017) treated a removal of spurious buckling modes which occur in optimal topology designs for multiple steel materials. Nguyen *et al.* (2018) proposed topology optimization computation of multi-materials CFRP for retrofitting the

*Corresponding author, Associate Professor

E-mail: dongkyulee@sejong.ac.kr

^aPh.D. student

E-mail: btthanhk11@gmail.com

^bPh.D. student

E-mail: xuannq.2309@gmail.com

^cPh.D.

E-mail: michael.herrmann@berkeley.edu

^dProfessor

E-mail: filippou@ce.berkeley.edu

concrete beam column joint with various cases of crack patterns by using multiple materials.

To discover the multi-material design distribution for plate-like structures, Goo *et al.* (2016) presented topology optimization for thin plate structures with bending stress constraints. A novel resizing algorithm of topology optimization for Mindlin-Reissner plate structures is studied by Belblidiaa *et al.* (2001). El-Sabbagh *et al.* (2008) investigated optimal topologies of plates with various periodic configurations by using Mindlin-Reissner plate theory. A novel deformation mechanism-based material model for topology optimization of laminated plates and shells considering large displacements is presented by Luo and Tong (2017). Binh and Lee (2019) presented multi-material topology optimization for Kirchhoff-Love thin plates with multi-directional variable thickness. Sun *et al.* (2019) proposed a new topology optimization approach for eigenfrequencies of uniform thickness plate via moving morphable components. As can be known, the real thick or thin plate structures may be defined in thickness dependence structures as well as widely used in engineering structures and machines. Moreover, the thick plate as a kind of plate models has a wider range of applicability, especially for mega structures, than the thin plate.

In this study, the optimal topological thick plate with variable thickness based on the Mindlin-Reissner plate theory (Reddy 2006, Zienkiewicz and Taylor 2005, Ferreira 2009) is proposed by using multi-material topology optimization approach. To eliminate shear locking phenomenon in Mindlin-Reissner plate theory, when plates are modeled by shear deformable elements, the mixed interpolation of tensorial components (MITC4) scheme (Bathe and Dvorkin 1985) is used. In addition, Winkler foundation parameter (Kobayashi and Sonoda 1989) is utilized to investigate the influence of variable thickness in multi-material optimal topological results.

The presented approach can be a useful design tool for engineers and designers in order to evaluate the mechanical and numerical interaction of variable thickness thick plates on Winkler foundations, in an attempt to achieve higher stiffness and provide lightweight as expected, within computational multi-material topology optimization. Moreover, by using multiple materials in a prescribed structure may take the best structural performance and lightweight within a mid-surface of variable thickness thick plate and explain how to provide stress-path reinforcement against damages and nonlinear behaviors of structures (Do and Filippou 2017, Crusells-Girona *et al.* 2017, Herrmann and Sobek 2017) and manufacture of mid-surface of variable thickness thick plate structures.

The rest of this study is organized as follows. The body of this paper is started in Section 2 with the analytical mathematical formulation of variable thickness thick plate relying on Winkler foundation. The approximate formulations by using finite element analysis and the formulation of MITC4 scheme are described in detail in Section 3. In Section 4, the model of multi-material topology problem including stiffness formulation, sensitivity analysis of compliance for structures are derived. As numerical examples, the optimal topological variable

thickness thick plates as well as the influence of the Winkler elastic foundation on results are discussed in Section 5. Finally, conclusions are drawn in Section 6.

2. Formulations of elasticity foundations of the variable thickness Mindlin-Reissner plate on Winkler foundation

According to Mindlin-Reissner plate theory (first order shear deformation plate theory), two-dimensional mid-surface $\Omega \in \mathbb{R}^2$, thickness $h(x, y)$ and transverse coordinate z are given. The deformation at any arbitrary point (x, y, z) is defined by the three-dimensional displacement vector defined by

$$\begin{aligned} u(x, y, z) &= z\phi_x(x, y), \\ v(x, y, z) &= z\phi_y(x, y), \\ w(x, y, z) &= w_0(x, y) \end{aligned} \quad (1)$$

where u, v are in-plane components of the displacement field in x and y Cartesian coordinate axes. w is the transverse (z) component of the displacement field and w_0 is the midplane deflection. ϕ_x and ϕ_y are the section rotation about y and x axes, respectively. They are shown in Fig. 1.

Strain fields are obtained using kinematic relations as follows.

$$\varepsilon = z\varepsilon_1, \quad \gamma = \varepsilon_2 \quad (2)$$

where

$$\varepsilon = \{\varepsilon_{xx} \quad \varepsilon_{yy} \quad \gamma_{xy}\}^T, \quad \gamma = \{\gamma_{xz} \quad \gamma_{yz}\}^T \quad (3a)$$

$$\varepsilon_1 = \{\phi_{x,x} \quad \phi_{y,y} \quad \phi_{x,y} + \phi_{y,x}\}^T \quad (3b)$$

$$\varepsilon_2 = \{\phi_x + w_{0,x} \quad \phi_y + w_{0,y}\}^T \quad (3c)$$

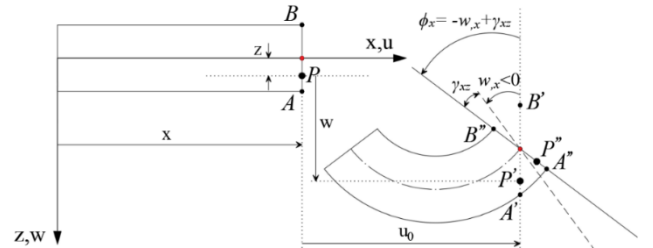


Fig. 1 Deformed plate cross section view

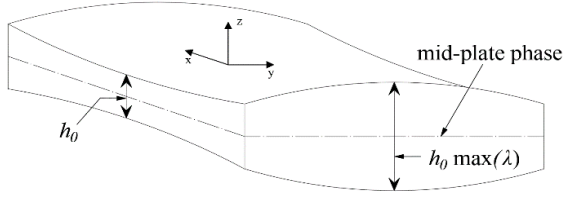


Fig. 2 Example of a multi-directional variable thickness plate

Based on a stress-strain law for the case when $\sigma_{zz} = 0$ for a homogeneous and isotropic plate with linear elastic material properties, the stresses can be determined as follows

$$\begin{Bmatrix} \sigma \\ \tau \end{Bmatrix} = \begin{bmatrix} \mathbf{Q}^b & 0 \\ 0 & \mathbf{Q}^s \end{bmatrix} \begin{Bmatrix} z\epsilon_1 \\ \epsilon_2 \end{Bmatrix} \quad (4)$$

where $\sigma = \{\sigma_{xx} \quad \sigma_{yy} \quad \sigma_{xy}\}^T$, $\tau = \{\tau_{xz} \quad \tau_{yz}\}^T$ and

$$\mathbf{Q}^b = \begin{bmatrix} Q_{11} & Q_{12} & 0 \\ Q_{21} & Q_{22} & 0 \\ 0 & 0 & Q_{66} \end{bmatrix}, \mathbf{Q}^s = \kappa \begin{bmatrix} Q_{44} & 0 \\ 0 & Q_{55} \end{bmatrix} \quad (5)$$

$$Q_{11} = Q_{22} = \frac{E}{1-\nu^2}, \quad Q_{12} = Q_{21} = \frac{\nu E}{1-\nu^2}, \quad (6)$$

$$Q_{44} = Q_{55} = Q_{66} = \frac{E}{2(1+\nu)}$$

where κ is the correction factor account for a parabolic variation of transverse shear stresses through a thickness of a given plate, it is chosen to be 5/6 in this study.

Constitutive relations for stress resultants are related to strains by the following relationships

$$M_{\alpha\beta} = \int_{-h/2}^{h/2} z\sigma_{\alpha\beta} dz, \quad S_\alpha = \int_{-h/2}^{h/2} \tau_{\alpha z} dz \quad (7)$$

where $\{\alpha, \beta\} = \{x, y\}$.

It is assumed to be multi-directional variable thickness as follows

$$h = h(x, y) = h_0 \lambda(x, y) \quad (8)$$

where h_0 is constant and $\lambda = \lambda(x, y)$ is not less than 1 as shown in Fig. 2. Therefore, the internal force resultants are obtained by integrals over the plate thickness in Eqs. (4), (7) and (8), as follows.

$$\begin{Bmatrix} \mathbf{M} \\ \mathbf{S} \end{Bmatrix} = \begin{bmatrix} [\mathbf{D}^b] & [0] \\ [0] & [\mathbf{D}^s] \end{bmatrix} \begin{Bmatrix} \epsilon_1 \\ \epsilon_2 \end{Bmatrix} \quad (9)$$

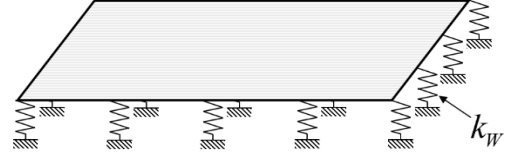


Fig. 3 Plate model embedded in elastic foundation presented by Winkler model

where $D_{ij}^b = \lambda^3 h_0^3 / 12 Q_{ij}^b$ and $D_{ij}^s = \kappa \lambda h_0 Q_{ij}^s$.

The virtual strain energy, i.e., the virtual work done by the applied transverse distributed load and the foundation reaction for a typical finite element Ω^e are denoted by δU , δV and δW_s , respectively, and given in detail below.

$$\begin{aligned} \delta U^e &= \int_{V^e} (\delta \epsilon^T \sigma + \delta \gamma^T \tau) dx dy dz \\ &= \int_{\Omega^e} (\delta \epsilon_1^T \mathbf{M} + \delta \epsilon_2^T \mathbf{S}) dx dy \\ &= \int_{\Omega^e} \{\delta \epsilon_1 \quad \delta \epsilon_2\} \{\mathbf{M} \quad \mathbf{S}\}^T dx dy \\ &= \int_{\Omega^e} \{\delta \epsilon_1 \quad \delta \epsilon_2\} \begin{bmatrix} [\mathbf{D}^b] & [0] \\ [0] & [\mathbf{D}^s] \end{bmatrix} \{\epsilon_1 \quad \epsilon_2\}^T dx dy \quad (10a) \end{aligned}$$

$$\begin{aligned} \delta V^e &= - \int_{\Omega^e} q_0 \delta w_0 dx dy, \\ \delta W_s^e &= k_w \int_{\Omega^e} w_0 \delta w_0 dx dy \quad (10b) \end{aligned}$$

where q_0 is the distributed transverse load and k_w is the Winkler modulus of subgrade reaction as shown in Fig. 3.

Now, the weak form of variable thickness Mindlin-Reissner plate on Winkler foundation problem is derived from the Hamilton's principle as

$$0 = \delta U + \delta V + \delta W_s \quad (11)$$

Substitution of the expressions obtained earlier for δU , δV and δW_s , results in

$$\begin{aligned} \sum_e \int_{\Omega^e} \left[\{\delta \epsilon_1 \quad \delta \epsilon_2\} \begin{bmatrix} [\mathbf{D}^b] & [0] \\ [0] & [\mathbf{D}^s] \end{bmatrix} \{\epsilon_1 \quad \epsilon_2\}^T \right. \\ \left. + (k_w w_0 - q_0) \delta w_0 \right] dx dy \\ = 0 \quad (12) \end{aligned}$$

3. Formulations of mixed interpolation of tensorial components (MITC4) scheme for variable thickness Mindlin-Reissner plates

3.1 Finite element analysis of variable thickness

Mindlin-Reissner plates

The generalized deflection and rotation of the plates using finite element method (FEM) can be approximated as follows.

$$\begin{aligned} \mathbf{u}^h &= \{w_0 \quad \phi_x \quad \phi_y\}^T = \sum_{i=1}^4 N_i \{w_i \quad \phi_{xi} \quad \phi_{yi}\}^T \\ &= \sum_{i=1}^4 N_i \mathbf{q}_i \end{aligned} \quad (13)$$

where N_i is the bilinear quadrilateral shape function

Substituting Eq. (13) into Eqs. (3) and (1), ones obtained

$$\begin{aligned} \boldsymbol{\varepsilon}_1 &= \sum_{I=1}^4 \begin{bmatrix} 0 & N_{I,x} & 0 \\ 0 & 0 & N_{I,y} \\ 0 & N_{I,y} & N_{I,x} \end{bmatrix} \begin{bmatrix} w_{0I} \\ \phi_{xI} \\ \phi_{yI} \end{bmatrix} \\ &= \sum_{I=1}^4 \mathbf{B}_I^b \mathbf{q}_I = \mathbf{B}^b \mathbf{q} \end{aligned} \quad (14a)$$

$$\begin{aligned} \boldsymbol{\varepsilon}_2 &= \sum_{I=1}^4 \begin{bmatrix} N_{I,x} & N_I & 0 \\ N_{I,y} & 0 & N_I \end{bmatrix} \begin{bmatrix} w_{0I} \\ \phi_{xI} \\ \phi_{yI} \end{bmatrix} \\ &= \sum_{I=1}^4 \mathbf{B}_I^s \mathbf{q}_I = \mathbf{B}^s \mathbf{q} \end{aligned} \quad (14b)$$

$$\begin{aligned} w_0 &= \sum_{I=1}^4 w_I N_I = \sum_{I=1}^4 [N_I \quad 0 \quad 0] \begin{bmatrix} w_{0I} \\ \phi_{xI} \\ \phi_{yI} \end{bmatrix} \\ &= \sum_{I=1}^4 \mathbf{B}_I^f \mathbf{q}_I = \mathbf{B}^f \mathbf{q} \end{aligned} \quad (14c)$$

where

$$\mathbf{B}^k = \begin{bmatrix} \mathbf{B}_1^k & \mathbf{B}_2^k & \mathbf{B}_3^k & \mathbf{B}_4^k \end{bmatrix}, \quad (15)$$

$$\mathbf{q} = [\mathbf{q}_1 \quad \mathbf{q}_2 \quad \mathbf{q}_3 \quad \mathbf{q}_4]^T, \quad k = \{b, s, f\}$$

Substituting Eq. (14) into Eq. (10), we have

$$\begin{aligned} \delta U^e &= \int_{\Omega^e} [\delta \boldsymbol{\varepsilon}_1^T \mathbf{D}^b \boldsymbol{\varepsilon}_1 + \delta \boldsymbol{\varepsilon}_2^T \mathbf{D}^s \boldsymbol{\varepsilon}_2] dx dy \\ &= \int_{\Omega^e} \delta \mathbf{q}^T (\mathbf{B}^{bT} \mathbf{D}^b \mathbf{B}^b + \mathbf{B}^{sT} \mathbf{D}^s \mathbf{B}^s) \mathbf{q} dx dy \quad (16a) \\ &= \delta \mathbf{q}^T \mathbf{K}_{bs}^e \mathbf{q} \end{aligned}$$

$$\delta V^e = - \int_{\Omega^e} \delta \mathbf{q}^T q_0 \mathbf{B}^{fT} dx dy = - \delta \mathbf{q}^T \mathbf{F}^e \quad (16b)$$

$$\begin{aligned} \delta W_s^e &= \int_{\Omega^e} \delta \mathbf{q}^T (\mathbf{B}^{fT} k_w \mathbf{B}^f) \mathbf{q} dx dy \\ &= \delta \mathbf{q}^T \mathbf{K}_w^e \mathbf{q} \end{aligned} \quad (16c)$$

Finally, the finite element model of static bending problems can be, respectively, expressed in the form of the following linear algebraic equations

$$\mathbf{K} \mathbf{q} = \mathbf{F} \quad (17)$$

where the stiffness matrix and applied load vector $\mathbf{K} = \mathbf{K}_{bs} + \mathbf{K}_w$ and \mathbf{F} can be expressed by element matrix components as follow.

$$\mathbf{K}^e = \int_{\Omega^e} \sum_{\varsigma=\{b,s,f\}} \mathbf{B}^{\varsigma T} \mathbf{D}^{\varsigma} \mathbf{B}^{\varsigma} dx dy \quad (18a)$$

$$\mathbf{F}^e = \int_{\Omega^e} q_0 \mathbf{B}^{fT} dx dy \quad (18b)$$

where $\mathbf{D}^f = \bar{k}_w D_{11}^b / l^4$ with \bar{k}_w is the dimensionless Winkler parameter.

3.2 Assumed MITC4 shear strain field

To eliminate shear locking phenomenon in Mindlin-Reissner plate theory, the shear energy is defined in terms of the assumed covariant transverse shear strain field of the MITC4 (Bathe and Dvorkin 1985, Thompson and Thangavelu 2002). In other words, the membrane-bending part is approximated as a standard analysis, but the approximation of the shear strains part has to be re-defined by the linear interpolation between mid-points of the element edges, namely that assume the transversal shear interpolation in local convective coordinates to be linear in

η direction for γ_ξ , and linear in ξ direction for γ_η as shown in Fig. 4.

$$\gamma_{\xi\eta} = \begin{Bmatrix} \gamma_\xi \\ \gamma_\eta \end{Bmatrix} = \frac{1}{2} \begin{Bmatrix} (1-\eta)\gamma_\xi^C + (1+\eta)\gamma_\xi^A \\ (1-\xi)\gamma_\eta^B + (1+\xi)\gamma_\eta^D \end{Bmatrix} \quad (19)$$

where the strain components at points A, B, C and D, can be directly evaluated from the displacement interpolations in Eq. (13) to obtain

$$\begin{aligned} \gamma_{\psi}^{\chi} &= x_{,\psi}^{\chi} (\beta_x^a + \beta_x^b) / 2 + y_{,\psi}^{\chi} (\beta_y^a + \beta_y^b) / 2 \\ &\quad + (w_a - w_b) / 2 \end{aligned} \quad (20)$$

where
 $(\chi, \psi, a, b) = \{(\xi, C, 2, 1), (\xi, A, 3, 4), (\eta, B, 4, 1), (\eta, D, 3, 2)\}$

By using MITC4 technique, the approximation of the modified shear strains components may be expressed as

$$\begin{aligned}\gamma^m &= \mathbf{J}^{-T} \gamma_{\xi\eta} \\ &= \mathbf{J}^{-T} \begin{bmatrix} \gamma_{\xi\eta}^1 & \gamma_{\xi\eta}^2 & \gamma_{\xi\eta}^3 & \gamma_{\xi\eta}^4 \end{bmatrix} \mathbf{q} = \mathbf{B}^m \mathbf{q}\end{aligned}\quad (21)$$

where

$$\gamma_{\xi\eta}^i = \begin{bmatrix} N_{i,\xi} & \xi_i x_{,\xi}^\chi N_{i,\xi} & \xi_i y_{,\xi}^\chi N_{i,\xi} \\ N_{i,\eta} & \eta_i x_{,\eta}^\psi N_{i,\eta} & \eta_i y_{,\eta}^\psi N_{i,\eta} \end{bmatrix}\quad (22)$$

in which

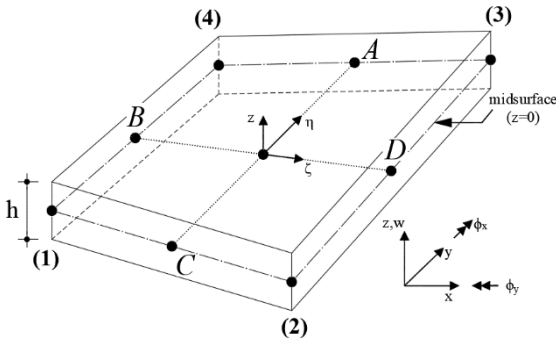
$(i, \chi, \psi) = \{(1, C, B), (2, C, D), (3, A, D), (4, A, B)\}$, $\mathbf{J} = \partial(x, y) / \partial(\xi, \eta)$ is Jacobian transformation matrix of the mapping $\mathbf{x} : [-1, 1]^2 \rightarrow \Omega^e$, i.e., where $\nabla_{\xi\eta}$ and ∇ stands for the gradient operators with respect to the $\xi - \eta$ and $x - y$ variables, respectively.

Finally, the element stiffness matrix in Eq. (18(a)) can be rewritten as follows

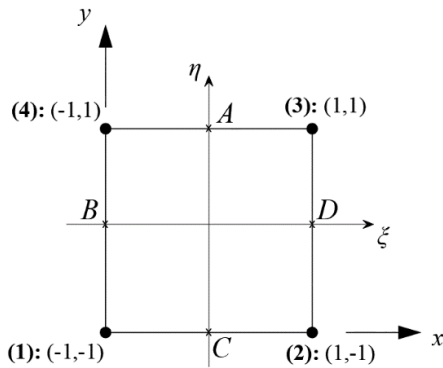
$$\mathbf{K}^e = \int_{\Omega^e} \sum_{\varsigma=\{b,m,f\}} \mathbf{B}^{\varsigma T} \mathbf{D}^{\varsigma} \mathbf{B}^{\varsigma} dxdy \quad (23)$$

where $\mathbf{B}^m = \mathbf{J}^{-T} \begin{bmatrix} \gamma_{\xi\eta}^1 & \gamma_{\xi\eta}^2 & \gamma_{\xi\eta}^3 & \gamma_{\xi\eta}^4 \end{bmatrix}$ and

$\mathbf{D}^m = \mathbf{D}^s$ are the modified derivative matrix and material property matrix of shear part, respectively.



(a) A general element in the $x - y$ plane



(b) A special element in the $x - y$ plane

Fig. 4 Geometry of quadrilateral plate element MITC4

4. Multi-material topology optimization model

According to the modified SIMP approach for multiple material (Tavakoli and Mohseni 2014), the relationship between Young modulus and multi-phase material density variable is expressed by

$$E(\rho) = \sum_{i=1}^{n+1} \rho_i^p E_i \quad (24)$$

where p is the penalization parameter. E_i and ρ_i denote for elastic Young's modulus and the material phase corresponding to phase i -th, respectively. n is number of non-void materials.

In this study, the alternating active phase algorithm proposed by Tavakoli and Mohseni (2014) is applied. In this algorithm, only two phases denoted as ' α ' and ' β ' are active at a time in each subproblem and the other phases are fixed. Therefore, in each subproblem of each computational step, the material properties for corresponding active phases needs to be used accordingly. Due to $\sum_{j=1}^{n+1} \rho_j = 1$, the evident formulation to intimate relationship between two active phases ' α ' and ' β ' at each location may written as follow.

$$\rho_\alpha + \rho_\beta = 1 - \sum_{i=1, i \neq \{\alpha, \beta\}}^{n+1} \rho_i \quad (25)$$

4.1 Optimization problem formulation

Analogous to the main ideal of standard topology optimization (TO) (Bendsøe and Kikuchi 1988), Multi-material topology optimization (MTO) aims to seek the optimum materials distribution to attain the maximum structural stiffness for multiple materials problem. In other words, MTO becomes a minimally total strain energy problem (objective function) of the given structure with a prescribed material volume under certain constraints. The general mathematical formulation of problem is written as follow.

$$\begin{aligned}\text{minimize : } & O(\rho_i, \mathbf{U}) = \mathbf{U}^T \mathbf{K} \mathbf{U} \\ \text{subject to : } & \mathbf{K}(\rho) \mathbf{U} = \mathbf{F} \\ & \int_{\Omega} \rho_i d\Omega \leq V_i \\ & 0 < \varepsilon_i \leq \rho_i \leq 1\end{aligned}\quad (26)$$

where C is compliance or objective function and ε_i is a very small lower bound non-zero value which to avoid singularities in computation. ρ_i and V_i are the density vector and volume fraction for phase material i -th with $i = \overline{1:n}$; \mathbf{U} , \mathbf{F} and \mathbf{K} are global load, displacement vector and global stiffness matrix, respectively.

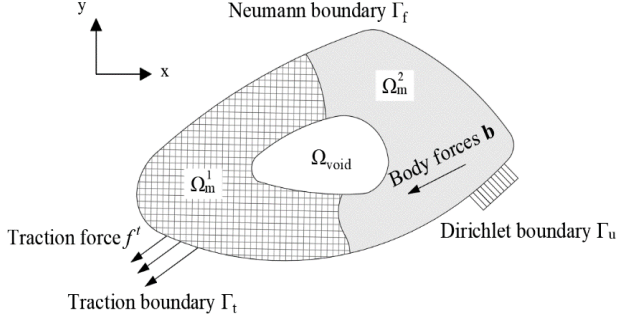


Fig. 5 Multi-material topology optimization design domain with voids and solids

4.2 Sensitivity formulation of mean compliance

The element stiffness matrix can be expressed through the use of Eqs. (23) and (24) as follows.

$$\mathbf{K}^e = \int_{\Omega^e} \sum_{t=1}^{n+1} \sum_{\varsigma=\{b,m,f\}} \rho_t^p \mathbf{B}^{\varsigma T} \mathbf{D}_{0t}^{\varsigma} \mathbf{B}^{\varsigma} dx dy \quad (27)$$

where \mathbf{D}_{0t}^k with $k = \{b, s, f\}$ is the material property matrix for an element with unit density corresponding to t -th phase. Finally, the sensitivity of objective function $C_{,\rho_\alpha} = \partial C / \partial \rho_\alpha$ and the material volume $V_{,\rho_\alpha} = \partial V / \partial \rho_\alpha$ in terms of multiple phase densities can be determined as follows.

$$C_{,\rho_\alpha} = -\mathbf{U}_e^T \mathbf{K}_{,\rho_\alpha}^e \mathbf{U}_e, \quad V_{,\rho_\alpha} = V^e \quad (28)$$

where the derivative component of element stiffness matrix component with respect to phase densities ' α ' can be calculated as follows.

$$\begin{aligned} \mathbf{K}_{,\rho_\alpha}^e &= \frac{\partial \mathbf{K}^e}{\partial \rho_\alpha} \\ &= p \rho_\alpha^{p-1} \int_{\Omega^e} \sum_{\varsigma=\{b,m,f\}} \rho_t^p \mathbf{B}^{\varsigma T} (\mathbf{D}_{0\alpha}^{\varsigma} - \mathbf{D}_{0\beta}^{\varsigma}) \mathbf{B}^{\varsigma} dx dy \end{aligned} \quad (29)$$

In order to safeguard of presence of result to topology optimization problem and to avoid the establishment of checkerboard patterns, a filtering technique on the resulting design is suggested (Bendsøe and Kikuchi 1988). The filtered sensitivity of compliance $C_{,\rho_\alpha}^f = \partial C^f / \partial \rho_\alpha$ and the multi-material volume $V_{,\rho_\alpha}^f = \partial V^f / \partial \rho_\alpha$ with respect to density of phase ' α ' of element ℓ -th can be displayed such as

$$C_{,\rho_\alpha}^f = \frac{\sum H_{ei} \rho_\alpha^i C_{,\rho_\alpha}^i}{\rho_\alpha \sum H_{ei}}, \quad V_{,\rho_\alpha}^f = \frac{\sum H_{ei} \rho_\alpha^i V^i}{\rho_\alpha \sum H_{ei}} \quad (30)$$

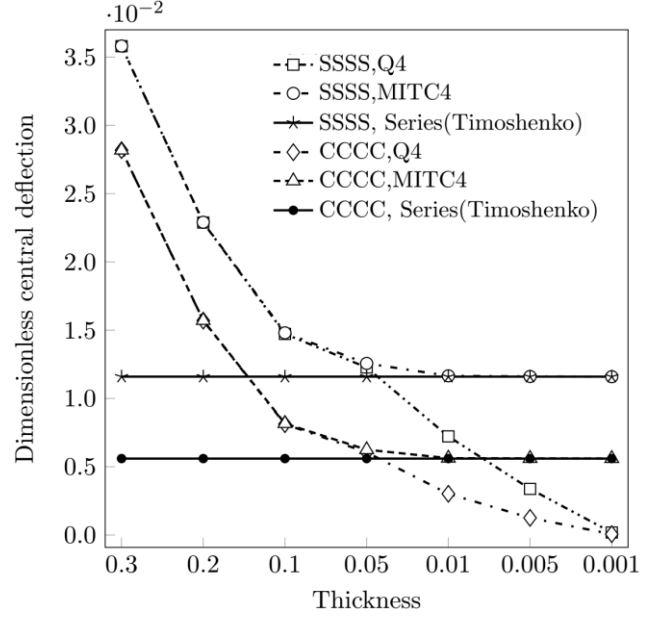


Fig. 6 The computed dimensionless central deflection of square thick plate in case central concentrated load, CCCC and SSSS boundaries

where $H_{ei} = r_{\min} - \text{dist}(e, \{f \in N \mid \text{dist}(e, f) \neq r_{\min}\})$ is a convolution operator with r_{\min} which is filter radius, $\text{dist}(e, f)$ is distance between the center of element ℓ and f .

5. Numerical examples and discussion

5.1 The benchmark solutions relying on thickness of Mindlin-Reissner plate theory

In other to verify the accuracy of models, the computed dimensionless central deflection of a square plate applied by central concentrated load is calculated under two boundary condition simply supported (SSSS) and clamped (CCCC) boundary conditions at four edge sides of the given thick plate. Through the change of the thickness, the present plate models are compared with the benchmark solutions is presented by Zienkiewicz and Taylor (2005) for thin square plate with the dimensionless central deflection for central concentrated load P , $\bar{w} = D_{11}^b w_{\text{central}} / q_0 l^2$.

As shown in Fig. 6, by using MITC4 scheme, when the thickness of the square plate becomes smaller, the value of dimensionless central deflection converges gradually on benchmark solutions for thin plate, but it does not match exactly original version by using the bilinear four-nodal rectangular (Q4) element thanks to shear locking problem. To show more clearly the influence of shear locking problem in MTO, the optimal topological results of thin plate by Mindlin-Reissner plate theory is compared with the classical plate theory (CPT), as shown in Figs. 7 and 8. Moreover, the sketched optimal topology plates by using

Table 1 Material properties of each material

Material properties	Number of materials		
	One (red)	Two (red, blue)	Three (red, blue and green)
Elastic modulus	$E_r^0 = 1$	$E_r^0 = 1, E_b^0 = 2$	$E_r^0 = 1, E_b^0 = 2, E_g^0 = 4$
Volume	$V_r = 50\%$	$V_r = 20\%, V_b = 30\%$	$V_r = 10\%, V_b = 15\%, V_g = 25\%$

MITC4 into isometric view (ISO view) are also presented. For the purpose, the plate is considered as a thin plate with the non-dimensional thickness 0.01 which is used uniformly. For convenience of obtaining optimal topological square plates, the total volume fraction is fixed to be 50% with plate dimension $l=1$, Poisson's ratio 0.3 is used, Young's modulus and volume fraction parameter for each material are presented in Table 1, with Young's modulus and volume fraction of void material are $E_v = 10^{-4}$ and $V_v = 1 - \sum_{k \neq v} V_k$, respectively.

As can be seen in Figs. 7 and 8, optimal topologies of Mindlin-Reissner plate theory by MITC4 scheme tend to be analogous to optimal topologies by CPT (Banh and Lee 2019) for both two kinds of boundary conditions. This once again demonstrates the use of MITC4 contributes to creating more comprehensive accuracy for Mindlin-Reissner plate theory when thin plate is considered, even in multi-material topology optimization problem. Moreover, the converged compliance in three material cases of both boundary conditions is shown in Fig. 9. The converged compliances in CCCC are always smaller than those of the SSSS. Then it leads to produce the optimal topologies of this boundary case which is stiffer mid-surface than remaining boundary condition.

5.2 The influence of variable thickness on optimal topologies of thick plate

In this Section, thick square plates with the variable thickness are considered through three cases of uniform thickness, linear variable thickness and multi-directional variable thickness as shown in Fig. 10. Mathematical formulations of the continuous variable thickness cases are written as follow to evaluate optimal topologies of a targeted internal mid-surface of given thick plates.

$$\text{Case 1: } h = 0.3 \quad (30a)$$

$$\text{Case 2: } h = 0.2(1+x) \quad (30b)$$

$$\text{Case 3: } h = 0.3(1+(x-0.5)^2 - (y-0.5)^2) \quad (30c)$$

Here, total volume of thick plates of the above cases is given to be all the same magnitudes with previous example, 50%. Note that three thickness functions are assumed on

Eq. (30) must ensure the unify the total volume of plate $V_0 = 0.3$.

Final optimal designs of three cases of mid-surface considering CCCC and SSSS is shown in Fig. 11. As can be seen, one of the most recognizable points in the results, regardless of uniform or non-uniform thickness and boundary conditions, is that the stiffest materials are always assigned near at the concentrated load in multi-material cases, followed by the effect of boundary condition positions. This shows the distribution of the current method tends to focus on strong stress concentration regions.

As the results, the symmetry of material density distribution over x- and both directions of case 2 and 3, respectively, is displayed quite clearly. Moreover, the stiff density distribution of both non-uniform thickness cases tends to allocate in places with thinner thicknesses. This contributes to demonstrate the influence of the variable thickness on material density distribution into optimal topological results. Furthermore, the compliance by using three materials is smaller than that by using one and two materials. It appeals that multi-material may produce stiffer structure even in variable thickness cases through appropriate proportion of material quantities.

The converged curves of objective function in three material cases of three different thickness cases are shown in Fig. 12.

5.3 The influence of Winkler parameter on optimal topologies of variable thickness thick plate

This example presents the influence of topology optimization results depending on the variable thickness thick square plate, when embedded in the Winkler foundation. The optimal topological thick plates presented in Figs. 13-15 show the variation of number of materials with respect to different values of dimensionless Winkler stiffness.

As can be seen, higher value of dimensionless Winkler parameter, the objective functions are lower. And the stiff material tends to focus in the concentrated load position when the Winkler parameter tends to be higher. In addition, higher dimensionless Winkler parameters produce more sensitive distribution of material densities for optimal topological thick plates. According to basic physical theory, when the higher value of Winkler parameter is, the stiffer of the foundation is. When Winkler parameter comes up to a

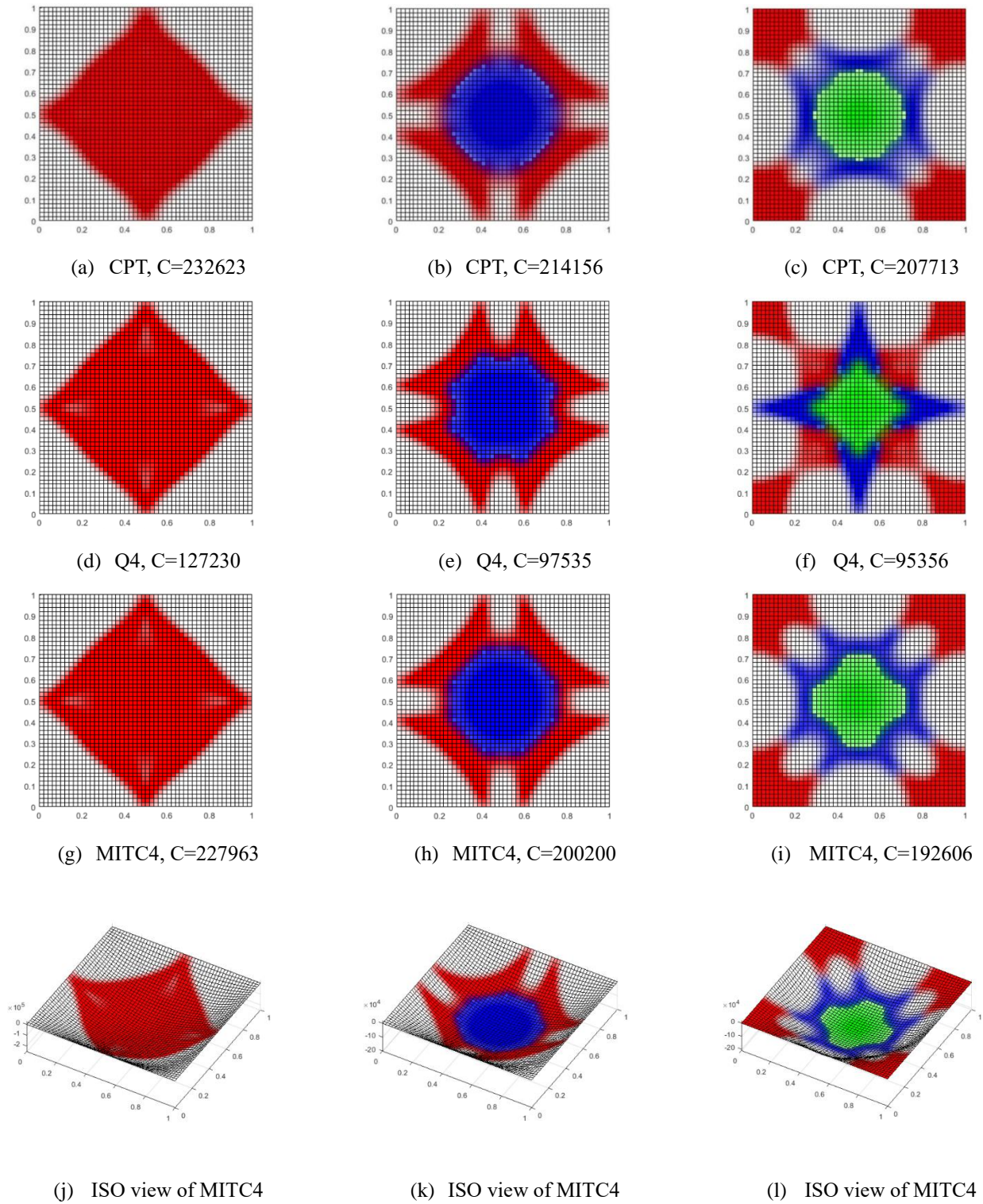


Fig. 7 Optimal topology configuration of a square thick plate for central concentrated load with the simply supported boundary condition (SSSS)

large number, the foundation behaves inelastic, in other words, it acts as a stiff foundation. Therefore, in the case of applying a concentrated load at the center of thick plates with the high Winkler parameter such as 4^4 and 5^4 , some optimal topological results do not tend to depend on

boundary conditions and the material densities only tend to be mainly distributed near the location of the concentrated load. Furthermore, in case of SSSS boundary condition with Winkler parameter value of 5^4 , optimal topological results of both case 1 and 3 are similar in terms of optimal topologies to converged value of objective function.

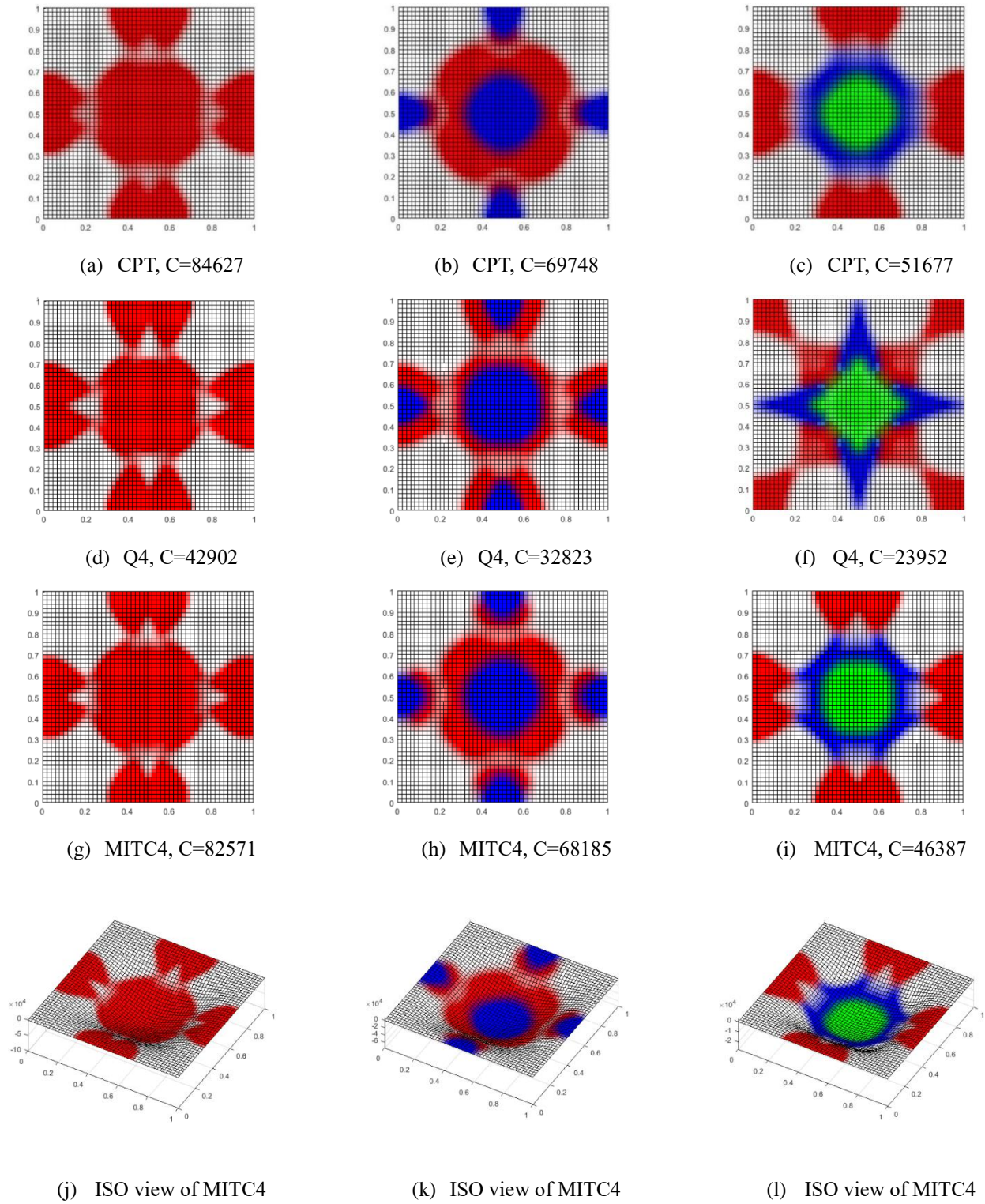


Fig. 8 Optimal topology configuration of a square thick plate for central concentrated load with the clamped boundary condition (CCCC)

The influence of various Winkler parameters with respect to different boundary conditions as well as different number of materials are depicted clearly in Fig. 16. As can be seen, the converged objective functions in all cases are descending along the ascending of Winkler parameters.

Besides, it once again demonstrates that by using more stiffer material with the same magnitudes of volume fraction, the multi-material topology optimization may produce stiffer structure, even when affected by variable thickness and Winkler foundation parameter.

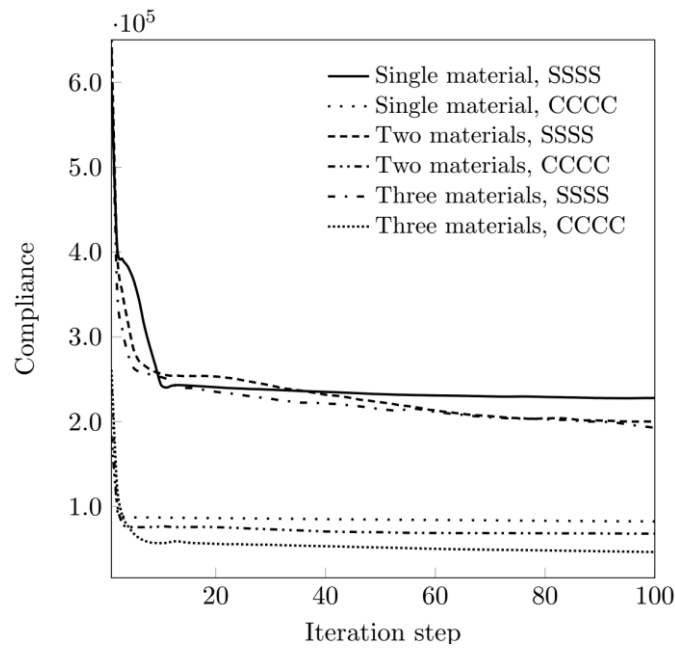
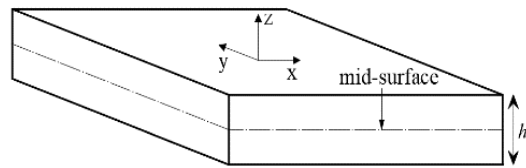
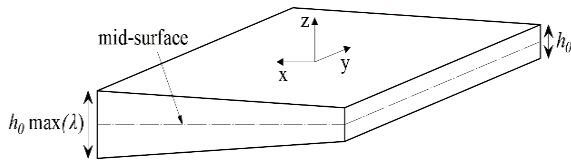


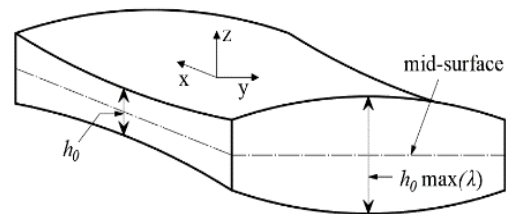
Fig. 9 Convergence histories of objective functions for thick plates under a concentrated load by using MITC4



Case 1: Uniform thickness



Case 2: Linear variable thickness



Case 3: Multi-directional nonlinear variable thickness

Fig. 10 Three dimensions variable thickness thick plate cases

6. Conclusions

In this study, computational multi-material topology optimization for searching optimal mid-surface configuration of variable thickness thick plate is proposed. Target structures based on Mindlin-Reissner plate theory relying on Winkler elastic foundation are contributed to the present topology optimization method. The mathematical formulations of compliance sensitivities of variable thickness as well as multi-material densities of plates by combining Mindlin-Reissner plate theory with MITC4 scheme and multi-material topology optimization method are derived in detail in this article. Three thickness cases:

uniform, linear and multi-directional nonlinear thickness are investigated. In addition, in case of multi-material topology optimization considering variable thickness thick plates, the influence of Winkler parameters on optimal topological results is also considered. Finally, optimal topological evaluation of visualizing mid-surface within variable thickness thick plate resting on Winkler foundation would be considered explicitly with respect to manufacturing products. Moreover, the present mid-surface topology design may be a reasonable in a use of real thick plates for the purpose of providing the feasibility and predictability to engineers and designers.

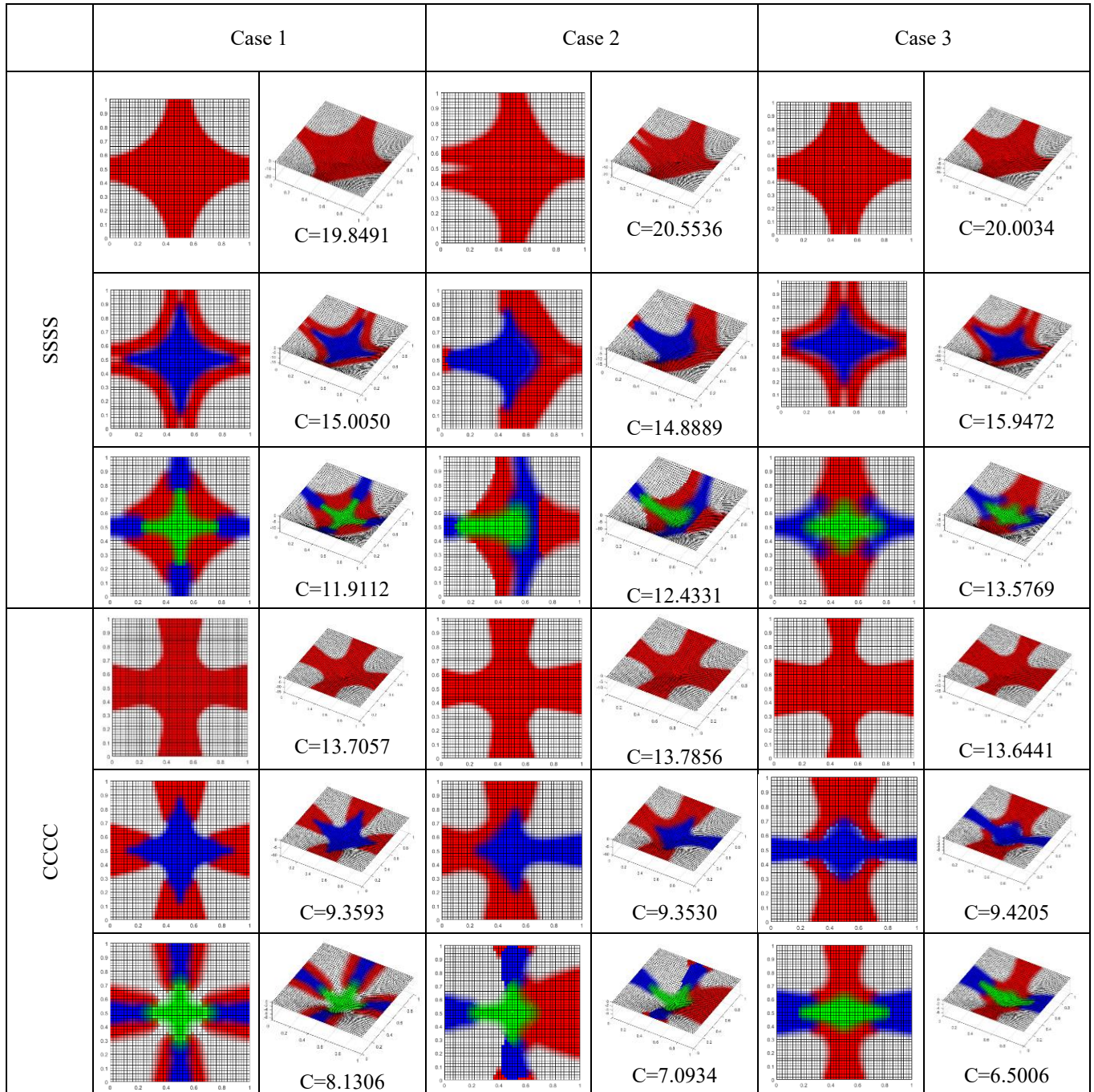
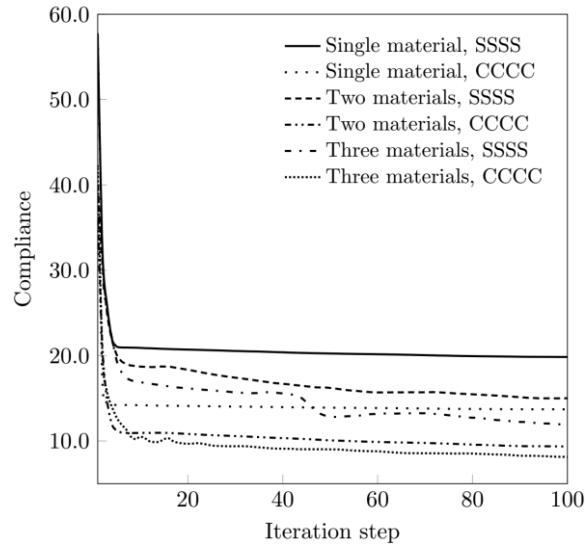
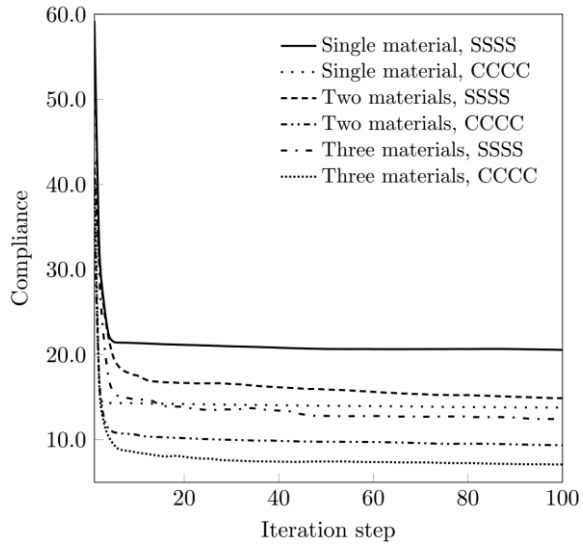


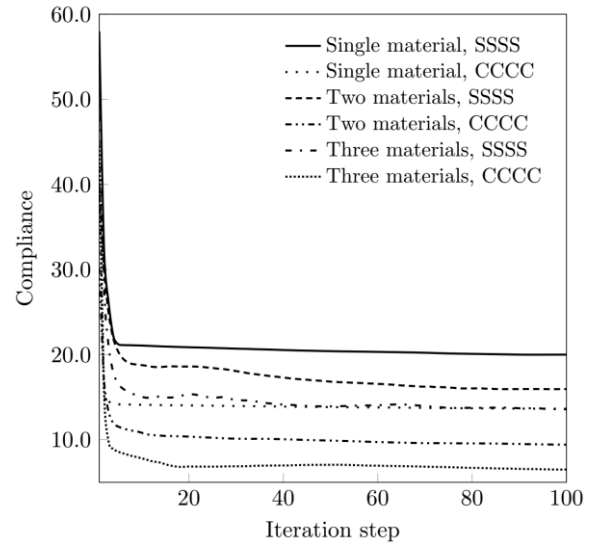
Fig. 11 Distributions of optimal topology material densities in mid-surface by using multiple various materials of two boundary conditions under a concentrated load



(a) Uniform thickness



(b) Linear variable thickness



(c) Multi-directional nonlinear variable thickness

Fig. 12 Convergence histories of objective functions for three cases variable thickness plates under a concentrated load

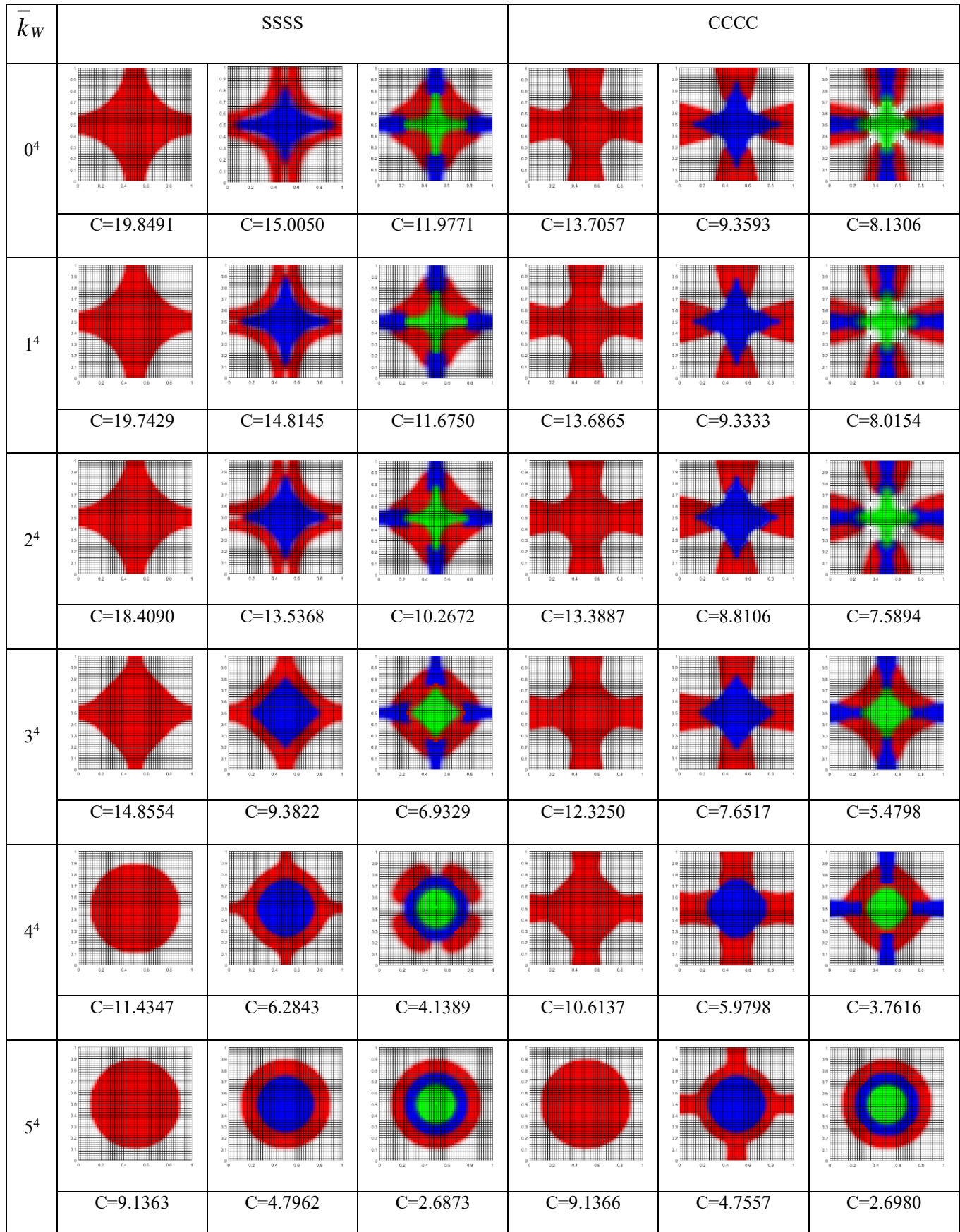


Fig. 13 Optimal topologies of Case 1: Uniform thickness

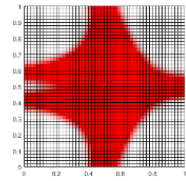
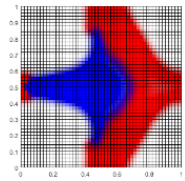
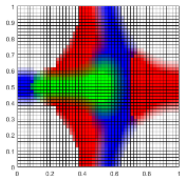
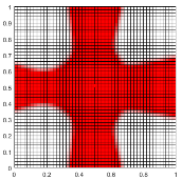
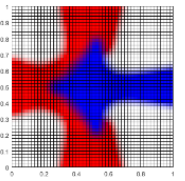
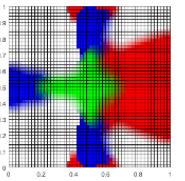
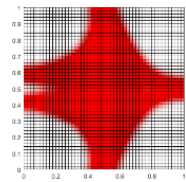
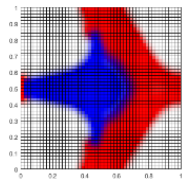
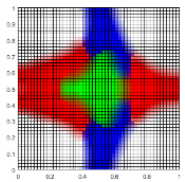
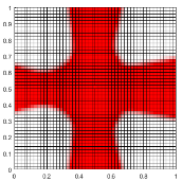
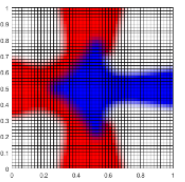
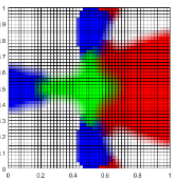
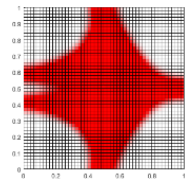
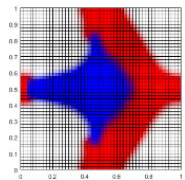
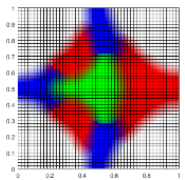
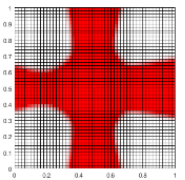
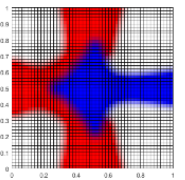
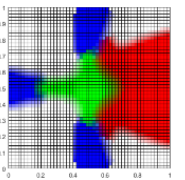
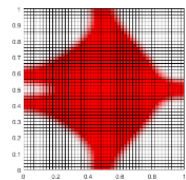
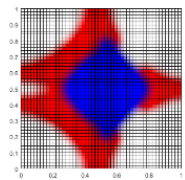
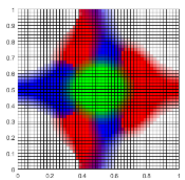
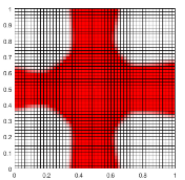
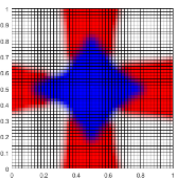
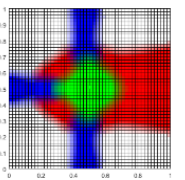
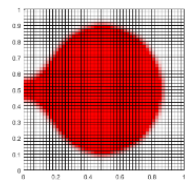
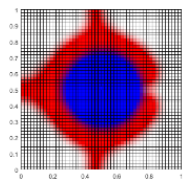
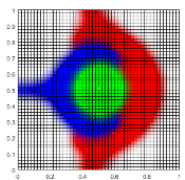
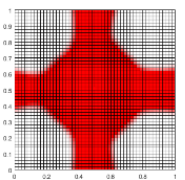
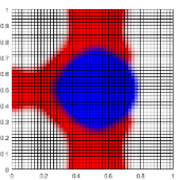
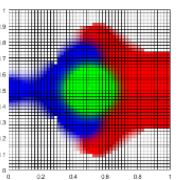
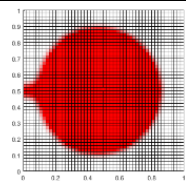
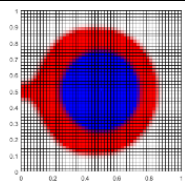
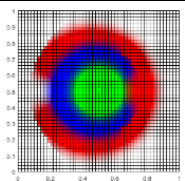
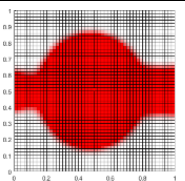
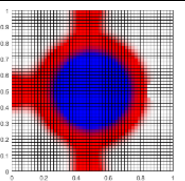
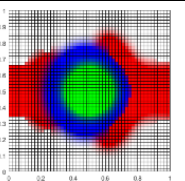
\bar{k}_w	SSSS			CCCC		
0^4						
	C=20.5336	C=14.8889	C=12.4331	C=13.7856	C=9.3530	C=7.0334
1^4						
	C=20.4799	C=14.7514	C=11.4347	C=13.7656	C=9.3098	C=7.0111
2^4						
	C=18.9919	C=13.4140	C=11.0396	C=13.4666	C=9.0267	C=6.6270
3^4						
	C=15.1869	C=9.9387	C=7.4503	C=12.3816	C=7.9450	C=5.6926
4^4						
	C=11.4412	C=6.5260	C=4.0783	C=10.6650	C=6.1155	C=3.9740
5^4						
	C=9.1852	C=4.8178	C=2.8433	C=9.1076	C=4.8348	C=2.7736

Fig. 14 Optimal topologies of Case 2: Linear variable thickness

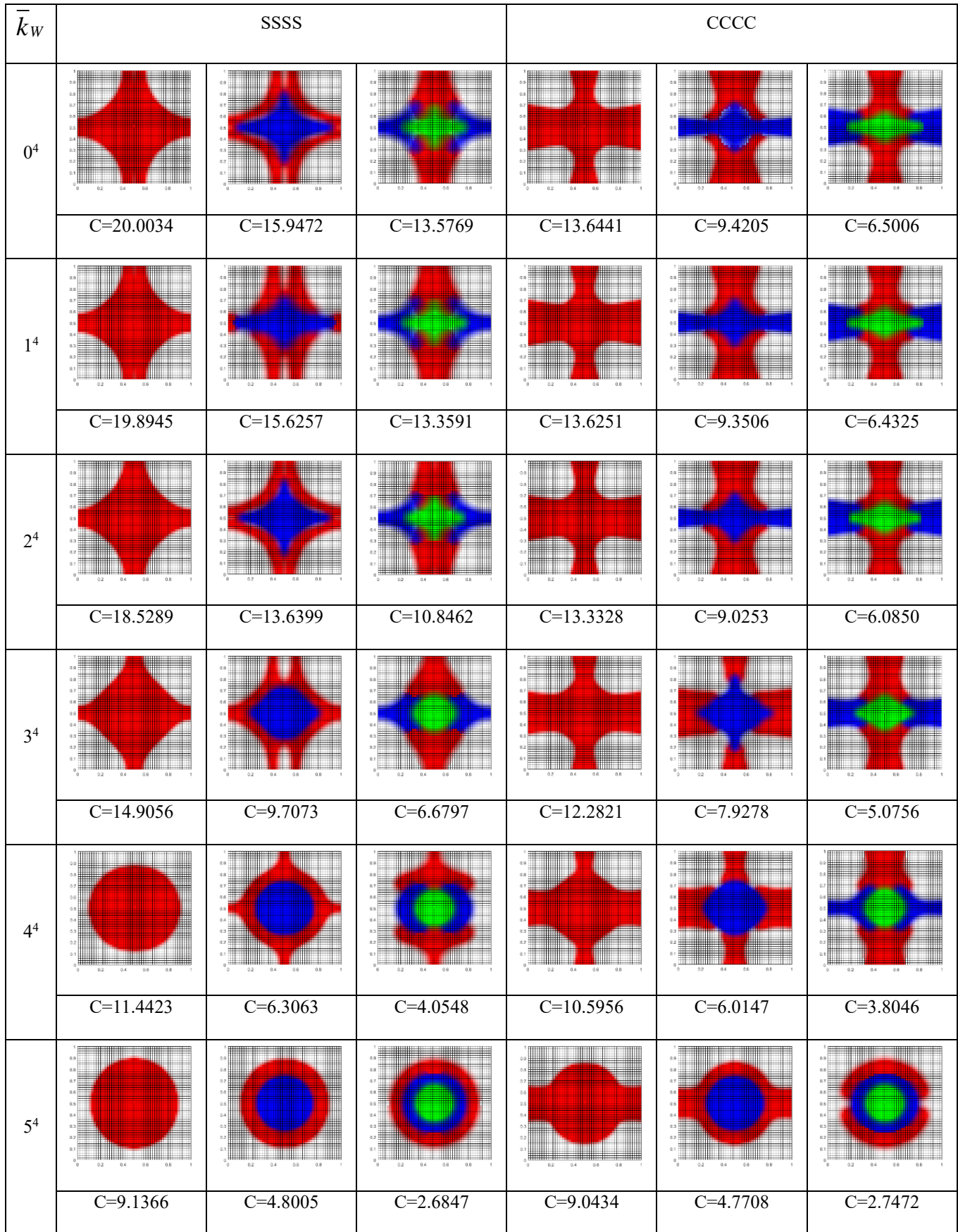


Fig. 15 Optimal topologies of Case 3: Multi-directional nonlinear variable thickness

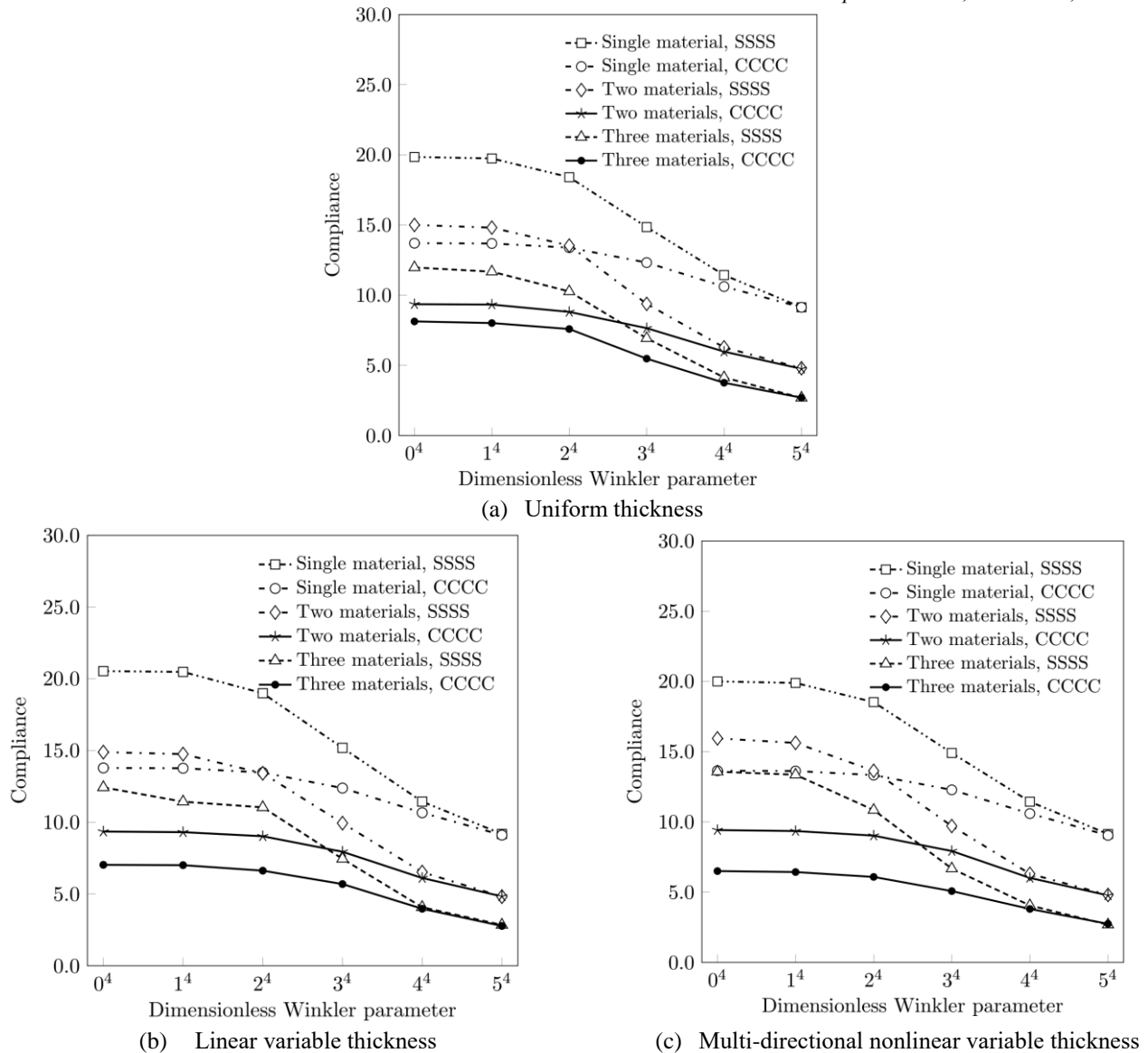


Fig. 16 Effects of the dimensionless Winkler parameter on optimal topologies in both boundary conditions
<https://doi.org/10.1007/s00158-018-2143-8>.

Acknowledgments

This research was supported by a grant (2017R1A2B4001960) from the National Research Foundation of Korea (NRF) & University of California, Berkeley visiting research scholar program from LG Yonam Foundation (of Korea).

This work was supported by the faculty research fund of Sejong University in 2019.

References

- Bagherinejad, M.H. and Haghollahi, A. (2018), "Topology optimization of steel plate shear walls in the moment frames", *Steel Compos. Struct.*, **29**(6), 771-783. <https://doi.org/10.12989/scs.2018.29.6.771>.
- Banh, T.T. and Lee, D. (2019), "Topology optimization of multi-directional variable thickness thin plate with multiple materials", *Struct. Multidiscip. O.*, **71**, 197-224. [http://dx.doi.org/10.1016/0045-7825\(88\)90086-2](http://dx.doi.org/10.1016/0045-7825(88)90086-2).
- Bathe, K.J. and Dvorkin, E. (1985), "A four node plate bending element based on Mindlin-Reissner plate theory and mixed interpolation", *Int. J. Numer. Method. Eng.*, **21**, 367-383. <https://doi.org/10.1002/nme.1620210213>.
- Belblidiaa, F., Lee, J.E.B., Rechakb. S. and Hinton, E. (2001), "Topology optimization of plate structures using a single- or three-layered artificial material model", *Adv Eng Softw.*, **32**(2), 159-168. [https://doi.org/10.1016/S0045-7949\(00\)00141-3](https://doi.org/10.1016/S0045-7949(00)00141-3).
- Bendsøe, M.P. and Kikuchi, N. (1988), "Generating optimal topologies in structural design using a homogenization method", *Struct. Multidiscip. O.*, **71**, 197-224. [http://dx.doi.org/10.1016/0045-7825\(88\)90086-2](http://dx.doi.org/10.1016/0045-7825(88)90086-2).
- Crusells-Girona, M., Filippou, F.C. and Taylor, R.L. (2017) "A mixed formulation for nonlinear analysis of cable structures", *Comput. Struct.*, **186**, 50-61. <https://doi.org/10.1016/j.compstruc.2017.03.011>.
- Doan, Q.H. and Lee, D. (2017), "Optimum topology design of multi-material structures with nonspurious buckling constraints", *Struct. Multidiscip. O.*, **71**, 197-224. [http://dx.doi.org/10.1016/0045-7825\(88\)90086-2](http://dx.doi.org/10.1016/0045-7825(88)90086-2).

- Adv. Eng. Softw.*, **114**, 110-120.
<https://doi.org/10.1016/j.advengsoft.2017.06.002>.
- El-Sabbagh, A., Akl, W. and Baz, A. (2008), "Topology optimization of periodic Mindlin plates", *Finite Elem. Anal. Des.*, **44**(8), 439-449. <https://doi.org/10.1016/j.finel.2008.01.016>.
- Ferreira, A.J.M. (2009), *The finite element method for solid and structural mechanics*, Springer Science Business Media B.V.
- Goo, S., Wang, S., Hyun, J. and Jung, J. (2016), "Topology optimization of thin plate structures with bending stress constraints", *Comput. Struct.*, **175**, 134-143.
<https://doi.org/10.1016/j.compstruc.2016.07.006>.
- Herrmann, M. and Sobek, W. (2017), "Functionally graded concrete: Numerical design methods and experimental test of mass-optimized structural components", *Struct. Concrete*, **18**, 54-66. <https://doi.org/10.1002/suco.201600011>.
- Kobayashi, H. and Sonoda, K. (1989), "Rectangular Mindlin plates on elastic foundations", *Int. J. Mech. Sci.*, **31**(9), 679-692.
[https://doi.org/10.1016/S0020-7403\(89\)80003-7](https://doi.org/10.1016/S0020-7403(89)80003-7).
- Lee, D. and Shin, S. (2016), "Evaluation of optimized topology design of cross-formed structures with a negative poisson's ratio", *Iran. J. Sci. Technol., Transact. Civil Eng.*, **40**(2), 109-120.
- Lieu, X.Q. and Lee, J. (2017), "A multi-resolution approach for multi-material topology optimization based on isogeometric analysis", *Comput. Method. Appl. M.*, **323**, 272-302.
<https://doi.org/10.1016/j.cma.2017.05.009>.
- Luo, Q. and Tong, L. (2017), "A deformation mechanism-based material model for topology optimization of laminated composite plates and shells", *Compos. Struct.*, **159**, 246-256.
<https://doi.org/10.1016/j.compstruct.2016.09.056>.
- Nguyen, P.A., Banh, T.T., Lee, D., Lee, J., Kang, J. and Shin, S. (2017), "Design of multiphase carbon fiber reinforcement of crack existing concrete structures using topology optimization", *Steel Compos. Struct.*, **29**(5), 625-645.
<https://doi.org/10.12989/scs.2018.29.5.635>.
- Reddy, J.N. (2006), *An introduction to the finite element method-Mc GrawHill*.
- Roodsarabi, M., Khatibinia, M. and Sarafrazi, S.R. (2016), "Hybrid of topological derivative-based level set method and isogeometric analysis for structural topology optimization", *Steel Compos. Struct.*, **21**(6), 1287-1306.
<https://doi.org/10.12989/scs.2016.21.6.1287>.
- Rozvany, G.I.N., Querin, O.M., Gaspar, Z. and Pomezanski, V. (2002), "Extended optimality in topology design", *Struct. Multidiscip. O.*, **24** (24), 257-261.
<https://doi.org/10.1007/s00158-002-0235-x>.
- Sigmund, O. and Torquato, S. (1997), "Design of materials with extreme thermal expansion using a three-phase topology optimization method", *J. Mech. Phys. Solids*, **45**, 1037-1067.
[https://doi.org/10.1016/S0022-5096\(96\)00114-7](https://doi.org/10.1016/S0022-5096(96)00114-7).
- Sun, J., Tian, Q., Hu, H. and Pedersen, N.L. (2019), "Topology optimization of eigenfrequencies of a rotating thin plate via moving morphable components", *J. Sound Vib.*, **448**, 83-107.
<https://doi.org/10.1016/j.jsv.2019.01.054>.